Available online at www.sciencedirect.com
SCIENCE DIRECT
Journal of Catalysis 226 (2004) 260–272
JOURNAL OF CATALYSIS
www.elsevier.com/locate/jcat

Effects of P_{H_2O}, P_{H_2S}, P_{H_2} on the surface properties of anatase–TiO_2 and γ-Al_2O_3: a DFT study

C. Arrouvel [a], H. Toulhoat [b], M. Breysse [c], P. Raybaud [a,*]

[a] *Division Chimie et Physico-Chimie Appliquées, Institut Français du Pétrole, 1-4 avenue de Bois-Préau, 92852 Rueil-Malmaison cedex, France*
[b] *Direction Scientifique, Institut Français du Pétrole, 1-4 avenue de Bois-Préau, 92852 Rueil-Malmaison cedex, France*
[c] *Laboratoire de Réactivité de Surface, UMR 7609 CNRS, Université Pierre et Marie Curie, 4 Place Jussieu, 75252 Paris cedex 05, France*

Received 6 February 2004; revised 7 May 2004; accepted 12 May 2004

Available online 2 July 2004

Abstract

Using density-functional theory combined with surface thermochemistry, the effects of sulfo-reductive conditions (P_{H_2O}, P_{H_2S}, P_{H_2}, and T), including those prevailing in the industrial process of hydrodesulfurization (HDS), are investigated for two catalytic supports: anatase–TiO_2 and γ-Al_2O_3. It is found that under the usual HDS conditions, H_2S may partially sulfide the (001) surface of anatase–TiO_2, leading to the formation of μ_2-S species together with two hydroxyl groups. The (110) surface of γ-Al_2O_3 is sulfided only if the water pressure is very low, leading to the formation of sulfhydryls and hydroxyls. The effect of H_2 pressure is also addressed. A comparison with published experimental data (such as TPR, IR, XPS) is supplied.

Keywords: Anatase–TiO_2; γ-Al_2O_3; Density-functional theory (DFT); Surface property; Morphology; Hydroxyls; Brønsted acidity; Hydrotreatment (HDT); Hydrodesulfurization (HDS); Infrared (IR)

1. Introduction

The catalyst used industrially in the hydrodesulfurization (HDS) process is made of a Co(Ni)MoS active phase dispersed on a γ-alumina support [1,2]. The strong effort devoted to the preparation and synthesis methods of γ-alumina has enabled the continuous improvement of its textural and acidic properties [3], making currently γ-alumina the preferred support for HDS catalysts. Besides, the anatase phase of TiO_2 has been the subject of many experimental works either as a model support itself [4–7] or in combination with alumina in a mixed phase [8,9]. Recent progress has been achieved in the preparation methods of anatase–TiO_2-based catalysts with higher specific areas and active-phase loadings [10], which offers new prospects for future industrial applications.

Besides the challenging task of developing a new class of industrial supports, it is of a fundamental interest to have a rational description of the support surface properties. Indeed, various support effects, not always understood, are involved in the prospect hydrotreating catalysts. For a detailed overview of support effects, the reader may refer to several articles [11,12]. A striking experimental result was reported by Ramirez et al. [4], revealing that the intrinsic HDS activity of anatase–TiO_2 supported MoS_2 is significantly higher than that of γ-alumina supported MoS_2. In order to explain this observation, many support effects have been suspected such as morphology effects, surface acidity [13], electronic effects [4], orientation [14], or even promotion by the support [7]. As a consequence, it is crucial to gain more insight into the surface properties (electronic, energetic, and structural) of supports as γ-alumina or anatase–TiO_2 under relevant working conditions.

The DFT approach is capable of establing the systematic atomistic characterization of the surface acidic and basic sites interacting with the active phase either in its precursor oxidic state or in the sulfided state. While DFT works have been devoted to the MoS_2 and Co(Ni)MoS active phases [15,16], less numerous theoretical studies have been devoted to the supports relevant for HDS catalysts, such as anatase–TiO_2 and γ-Al_2O_3. For that purpose, we have recently un-

* Corresponding author. Fax: +33 1 47 52 70 58.
E-mail address: pascal.raybaud@ifp.fr (P. Raybaud).

0021-9517/$ – see front matter
doi:10.1016/j.jcat.2004.05.019

dertaken a systematic DFT investigation of the bulk and surface properties of various oxides relevant for HDS catalysts: boehmite (AlOOH) [17], and other aluminum hydrooxides [18], γ-Al_2O_3 [19,20], and anatase–TiO_2 [21]. The DFT works by Digne et al. [20,22] and Arrouvel et al. [21] allow a consistent comparison of the two supports γ-Al_2O_3 and TiO_2, regarding the surface hydration process and the type of acidic and basic surface sites as a function of T and P_{H_2O}. These studies already put forward different features of the hydroxyl types and concentrations connected with the surface acidity. However, to further explore the chemical behavior of the two supports under sulfo-reductive conditions, such as those used in HDS, it is mandatory to take into account the influence of P_{H_2S} and P_{H_2}.

In the literature, a few experimental studies focused on the effects of H_2S on the γ-Al_2O_3 and anatase–TiO_2 supports. Among the techniques used to better characterize the surface state of the two supports in interaction with H_2S, we can refer to thermogravimetry measurements [23], calorimetry measurement [24], infrared (IR) spectroscopy [25–29], temperature-programmed desorption (TPD) [27], and sulfur isotope exchange [30]. In particular, Travert et al. [25] have carried out a rather exhaustive IR study on various oxides (including γ-Al_2O_3 and anatase–TiO_2). They gave an interesting analysis of the way H_2S may interact with the surface and irreversibly perturbs the high-frequency region of the IR spectra. A recent X-ray photoelectron spectroscopy (XPS) [7] revealed that anatase–TiO_2 becomes partially sulfided in the presence of H_2S and at T above 673 K, whereas earlier works [27,31] only revealed the reversible H_2S adsorption (molecular bonded) on anatase–TiO_2 whatever the temperature may be. In the case of γ-Al_2O_3, it seems possible to adsorb irreversibly H_2S and to form Al–SH species according to [23,26,29,32]. In particular, Okamoto et al. [32] estimated that the nondissociative adsorption energy of H_2S on γ-Al_2O_3 is about -54 kJ/mol, while the dissociative mode is about -142 kJ/mol.

To our knowledge, very few theoretical studies are devoted to the adsorption of H_2S on the two supports. Even fewer studies are devoted to the effect of P_{H_2} on γ-Al_2O_3 and on anatase–TiO_2. The density-functional study by Selloni et al. [33] investigated the adsorption energy of one H_2S molecule on the (101) surface of anatase–TiO_2. Two other works [34,35] investigated the adsorption of one H_2S molecule on the γ-Al_2O_3 surface modeled as a defective spinel. However, these works suffer from some weaknesses regarding first the structural representation of γ-Al_2O_3. Then, the hydration state of the support is not considered. Finally, the real chemical potential of sulfur is not taken into account in order to bridge the gap between the 0 K DFT-simulation and experimental conditions in terms of T, P_{H_2O}, P_{H_2S}, and P_{H_2}.

The aim of our study is thus to fill in the lack of theoretical insights on the effect of the sulfo-reductive conditions on the relevant surfaces exposed by anatase–TiO_2 and γ-Al_2O_3. For that purpose, we use the density-functional theory (DFT) coupled with a thermodynamic model, as defined in the next section. In Sections 3.1 and 3.2, the effect of P_{H_2S} on anatase–TiO_2 and γ-Al_2O_3 will be addressed, respectively. Section 3.3 is devoted to the effect of P_{H_2} on both supports. Finally in the discussion section, we propose an interpretation of our theoretical results in comparison with published experimental data (TPR, XPS, IR). The present work pays attention to the consistent comparison of the surface chemical properties of the two supports as a function of the working conditions (P_{H_2O}, P_{H_2S}, P_{H_2}, and T).

2. Methods

2.1. DFT calculations

Total energy calculations are performed within the density functional theory and the generalized gradient approximation (GGA) of Perdew and Wang [36]. To solve the Kohn–Sham equations, we used the Vienna ab initio Simulation Package (VASP) [37–39]. VASP performs an iterative diagonalization of the Kohn–Sham Hamiltonian via unconstrained band-by-band minimization of the norm of the residual vector to each eigenstate and via optimized charge-density mixing routines. The convergence criterion for the electronic self-consistent cycle is fixed at 0.1 meV per cell. The eigenstates of the electron wave functions are expanded on a plane-waves basis set using pseudopotentials to describe the electron–ion interactions within the projector augmented waves (PAW) approach [40]. For total energy calculations, we use a cutoff energy of 323.4 eV. The optimization of the atomic geometry at 0 K is performed by determining the exact Hellman–Feynman forces acting on the ions for each optimization step and by using a conjugate gradient algorithm. A full relaxation of all atomic positions in the cell is performed till the convergence criterion on the energy (0.1 meV/cell) is reached.

The OH-stretching modes are calculated within the harmonic approximation with a cutoff energy of 323.4 eV and the Hessian matrix is calculated by a finite difference approach, with a moving step size of ± 0.005 Å around the equilibrium position. The coupling with the first outmost layer of the surface is considered. The anharmonicity corrections for the OH stretching are performed following the method proposed by Lindberg [41] as implemented in the ANHARM program [42,43]. In this case, the interval of atomic dispacement is increased to $[-0.3, +0.4$ Å$]$. This approach has been fruitfully applied in [17] for determining the OH frequency calculations on boehmite surfaces. The anharmonicity correction ($w_e x_e$) calculated by this approach is between 71 and 73 cm^{-1} depending on the type of hydroxyl group and 44 cm^{-1} for sulfhydryl groups in the case of anatase–TiO_2, 47 cm^{-1} for sulfhydryl groups in the case of γ-Al_2O_3.

2.2. Surface energy calculations

We use the same method as already proposed in our previous works [20–22] to calculate the surface energy, Γ_{hkl}, for a given crystal orientation (hkl) and as a function of the working conditions fixed by temperature (T), water pressure (P_{H_2O}), hydrogen sulfide pressure (P_{H_2S}) and hydrogen pressure (P_{H_2}). Following the same formalism as in [21], the surface energy can be written as

$$A_{hkl}\Gamma_{hkl} = G(\mathrm{surf}_{hkl} + n_o H_2O + n_s H_2S + n_h H_2) - G(\mathrm{bulk}) - n_o\mu_{H_2O} - n_s\mu_{H_2S} - n_h\mu_{H_2}, \quad (1)$$

where $G(\mathrm{surf}_{hkl}+n_oH_2O+n_sH_2S+n_hH_2)$ is the free Gibbs energy of the surface (hkl) with n_o adsorbed water molecules, n_s adsorbed hydrogen sulfide molecules, n_h adsorbed hydrogen molecules for the surface area A_{hkl}. $G(\mathrm{bulk})$ is the free Gibbs energy of the bulk normalized to the number of atoms used in the supercell of the hydrated TiO_2 surface or the γ-Al_2O_3 surface. μ_{H_2O} (resp. μ_{H_2S}, μ_{H_2}) stands for the chemical potential of water (resp. of hydrogen sulfide and hydrogen).

Neglecting the variation of entropy for the condensed phases and the pV terms, as well as thermal variations of internal energies, the surface energy of the (hkl) facet can be expressed as follows,

$$\Gamma_{hkl} = \Gamma^0_{hkl} + \theta_{hkl}E_{ads} - \theta^{H_2O}_{hkl}\Delta\mu_{H_2O} - \theta^{H_2S}_{hkl}\Delta\mu_{H_2S} - \theta^{H_2}_{hkl}\Delta\mu_{H_2}, \quad (2)$$

where Γ^0_{hkl} stands for the surface energy in vacuum (i.e., without any adsorbed molecules).

$\theta^{H_2O}_{hkl}$ (resp. $\theta^{H_2S}_{hkl}$ and $\theta^{H_2}_{hkl}$) is the surface coverage of n_o-adsorbed H_2O molecules (resp. H_2S and H_2), meaning that

$$\theta^{H_2O}_{hkl} = \frac{n_o}{A_{hkl}} \quad \left(\text{resp.} \quad \theta^{H_2S}_{hkl} = \frac{n_s}{A_{hkl}}, \quad \theta^{H_2}_{hkl} = \frac{n_h}{A_{hkl}}\right).$$

In all what follows (including figures and tables), the unit for $\theta^{H_2O}_{hkl}$ (resp. $\theta^{H_2S}_{hkl}$ and $\theta^{H_2}_{hkl}$) is expressed in H_2O molecules (resp. H_2S and H_2) per nm^2. θ_{hkl} is the sum of the coverages of all adsorbed species.

E_{ads} is defined as the mean adsorption energy of n molecules ($n = n_o + n_s + n_h$):

$$E_{ads} = \left[E_{0K}(\mathrm{surf}_{hkl} + n_oH_2O + n_sH_2S + n_hH_2) - E_{0K}(\mathrm{surf}_{hkl}) - n_oe_{H_2O} - n_se_{H_2S} - n_he_{H_2}\right]/n. \quad (3)$$

$\Delta\mu_{H_2O}$ (resp. $\Delta\mu_{H_2S}$ and $\Delta\mu_{H_2}$) stands for the chemical potential of H_2O (resp. H_2S and H_2) with the internal energy of the isolated molecule, e_{H_2O} (resp. e_{H_2S} and e_{H_2}) as reference:

$$\Delta\mu_{H_2O} = h^0_{H_2O} - Ts^0_{H_2O} + RT\ln\left(\frac{p_{H_2O}}{p^0}\right) - e_{H_2O}, \quad (4)$$

$$\Delta\mu_{H_2S} = h^0_{H_2S} - Ts^0_{H_2S} + RT\ln\left(\frac{p_{H_2S}}{p^0}\right) - e_{H_2S}, \quad (5)$$

$$\Delta\mu_{H_2} = h^0_{H_2} - Ts^0_{H_2} + RT\ln\left(\frac{p_{H_2}}{p^0}\right) - e_{H_2}. \quad (6)$$

We will also use the notation θ^{OH}_{hkl} (resp. θ^{SH}_{hkl}, θ^{S}_{hkl}) for the surface coverage of formed OH groups (resp. SH, S) during the adsorption process.

The typical HDS conditions are defined for T between 600 and 700 K, as low P_{H_2O} (< 0.01 bar), $P_{H_2S} \sim 1$ bar, and P_{H_2} up to 30 bar (i.e., $P_{H_2S}/P_{H_2} \sim 5\%$). However, as it is difficult to precisely control P_{H_2O} under reaction conditions, it might be of interest to extend the range of (T, P) conditions. Hence, even if our main concern is for HDS conditions (as defined previously), all surface energies are calculated in a wider range of temperature (between 400 and 900 K) and water partial pressure (between 10^{-5} and 1 bar).

3. Results

3.1. Effect of P_{H_2S} on the anatase–TiO_2 surfaces

3.1.1. (101) surface

We know from our recent work [21] that the (101) surface is dehydrated at $P_{H_2O} = 0.01$ bar, between 400 and 900 K. The adsorption energies for various surface coverages of water, reported in Fig. 1, remain in the range of −79 to −69 kJ/mol, exhibiting a slight stabilizing effect for high coverages. The adsorption energy of H_2S on the same surface reveals that adsorption energies are significantly reduced with respect to H_2O. For instance, the adsorption energy of the first H_2S molecule is −37 kJ/mol in agreement with the value reported by Selloni et al. [33]. The adsorption configuration of H_2S is given in the inset of Fig. 1 for $\theta^{H_2S}_{101} = 1.3$ H_2S/nm^2. We have also tested the sulfidation of the surface, leading to a μ_2-S and a chemisorbed H_2O molecule. However, the resulting adsorption energy (−30 kJ/mol) is less favorable due to an endothermic substitution process (+44 kJ/mol) of one O atom by one S atom. Since in the layered TiS_2 structure [44], sulfur atoms are 3-fold coordinated, we have investigated the formation of μ_3-S species by substituting μ_3-O atoms by S. However, this configuration is even less stable. The significantly larger Ti–Ti distances on the (101) surface than on TiS_2 explain that the local structure constraints together with the energy cost for removing μ_3-O atoms make the sulfidation highly unfavorable.

Upon an increase of H_2S coverage, the adsorption energy decreases to −20 kJ/mol due to strong lateral repulsive interactions between H_2S molecules. Mixed coverages combining the simultaneous adsorption of H_2O and H_2S, as indicated by the circles and crosses in Fig. 1, show that the presence of H_2S has always a destabilizing effect. As a consequence, the surface energy diagram (Fig. 2) for low $P_{H_2O} \sim 10^{-2}$ bar and $P_{H_2S} = 1$ bar shows that the (101) surface does not contain any S species on a wide range of temperature. For T above 400 K, the adsorption of H_2S would require nonrealistic values of partial pressure of H_2S. Therefore, under working conditions, the (101) surface exposes

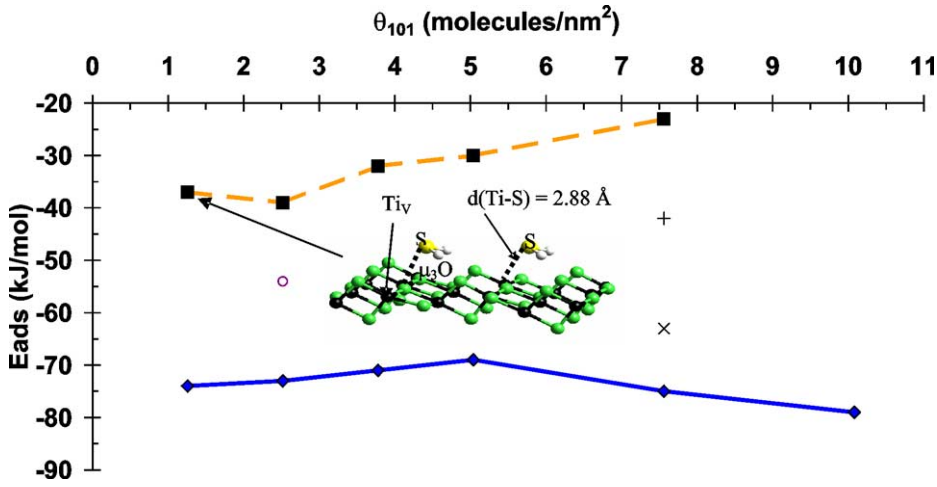

Fig. 1. Adsorption energies of H_2O (thick line) and H_2S (dashed line) on the (101) surface of anatase–TiO_2 as a function of the coverage. (■) $\theta_{101}^{H_2S} = \theta_{101}$ and $\theta_{101}^{H_2O} = 0$ (pure H_2S); (○) $\theta_{101}^{H_2S} = 1.3$ H_2S/nm^2 and $\theta_{101}^{H_2O} = 1.3$ H_2O/nm^2; (+) $\theta_{101}^{H_2S} = 5.0$ and $\theta_{101}^{H_2O} = 2.5$; (×) $\theta_{101}^{H_2S} = 2.5$ and $\theta_{101}^{H_2O} = 5.0$; (◆) $\theta_{101}^{H_2S} = 0$ and $\theta_{101}^{H_2O} = \theta_{101}$ (pure H_2O). Inset: ball and stick representation of the nondissociative adsorption of H_2S on the (101) surface of anatase–TiO_2 for $\theta_{101}^{H_2S} = 1.3$ H_2S/nm^2. (Black balls, Ti; small gray balls, O; large gray balls, S; white balls, H.)

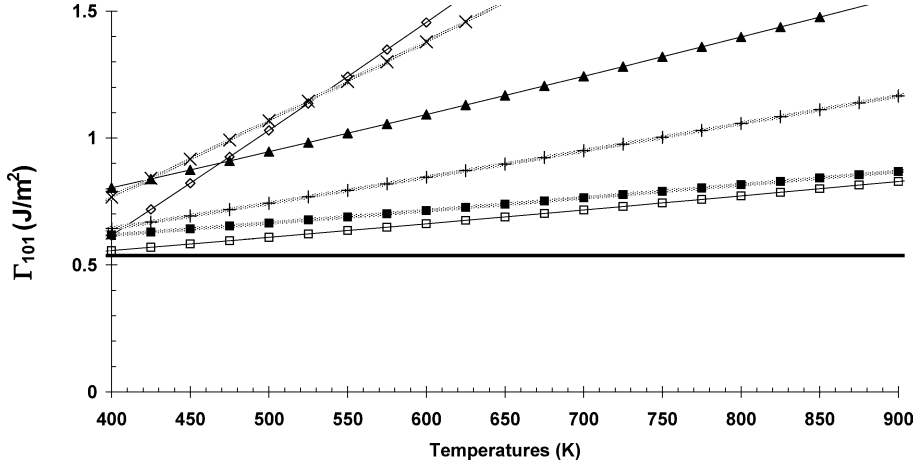

Fig. 2. Surface energy of the (101) surface of anatase–TiO_2 as a function of temperature for different coverages of H_2O and H_2S, $P_{H_2O} = 10^{-2}$ and $P_{H_2S} = 1$ bar. (—) $\theta_{101} = 0.0$ molecule/nm^2; (□) $\theta_{101}^{H_2O} = 1.3$ H_2O/nm^2; (◇) $\theta_{101}^{H_2O} = 10.1$; (■) $\theta_{101}^{H_2S} = 1.3$ H_2S/nm^2; (▲) $\theta_{101}^{H_2O} = 3.8$; (+) $\theta_{101}^{H_2O} = 1.3$ and $\theta_{101}^{H_2S} = 1.3$; (×) $\theta_{101}^{H_2O} = 2.5$ and $\theta_{101}^{H_2S} = 5.0$. (See text for definition and unit of θ_{101}.)

mainly μ_2-O and μ_3-O basic Lewis sites, and Ti_V acidic sites, without any S species.

3.1.2. (001) surface

As shown in [21], this surface remains hydrated at high temperatures even for low water partial pressure. In Fig. 3, the high adsorption energies of water (from −165 up to −101 kJ/mol) were explained by the high reactivity of the surface active sites, enabling the dissociative adsorption of water. When considering the H_2S adsorption, it appears that the reactivity for H_2S is enhanced. At low coverage ($\theta_{001} = 1.7$ molecule/nm^2), H_2S is even more strongly adsorbed than water with a resulting energy of −184 kJ/mol. As shown by the local structure for $\theta_{001} = 1.7$ (inset of Fig. 3) the surface is sulfided, and H_2S is totally dissociated, leading to the substitution of one μ_2-O atom by one μ_2-S species. This substitution implies the formation of two neighboring hydroxyl groups similar to those formed upon hydration of the surface. The two Ti–S distances are about 2.35 Å, and the Ti–S–Ti angle is 119°.

As observed for the (101) surface, a further increase of the H_2S coverage leads to a significant decrease of adsorption energy due to steric constraints between neighboring μ_2-S species. It is also worth noting that the variation of adsorption energies with H_2S coverage is significantly larger (about 140 kJ/mol) on this surface than on the (101) surface. This observation was already valid for water [21]. Mixed coverages, involving the simultaneous adsorption of H_2O and H_2S, reveal a destabilization of S species. This means that increasing the water partial pressure induces the release of adsorbed S species.

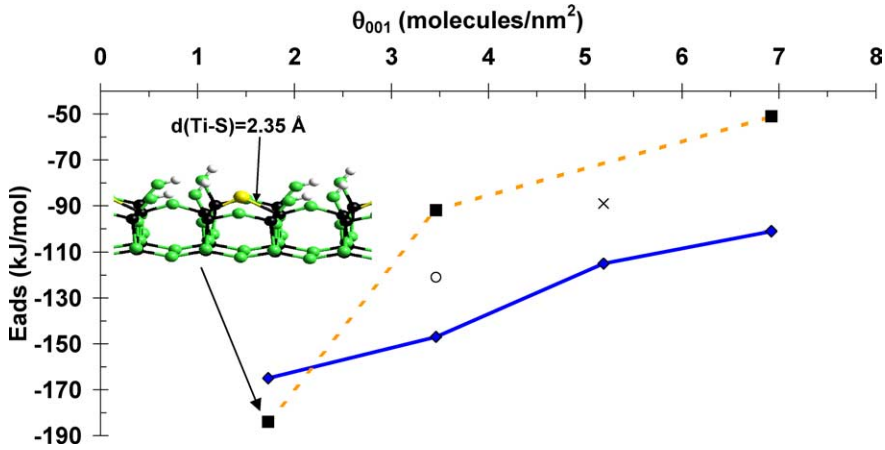

Fig. 3. Adsorption energies of H_2O (thick line) and H_2S (dashed line) on the (001) surface of anatase–TiO_2 as a function of the coverage. (■) $\theta_{001}^{H_2S} = \theta_{001}$ and $\theta_{001}^{H_2O} = 0$ (pure H_2S); (×) $\theta_{001}^{H_2S} = 1.7$ H_2S/nm^2 and $\theta_{001}^{H_2O} = 3.5$ H_2O/nm^2; (○) $\theta_{001}^{H_2S} = 1.7$ and $\theta_{001}^{H_2O} = 1.7$; (◆) $\theta_{001}^{H_2S} = 0$ and $\theta_{001}^{H_2O} = \theta_{001}$ (pure H_2O). (Same color coding as in Fig. 1.)

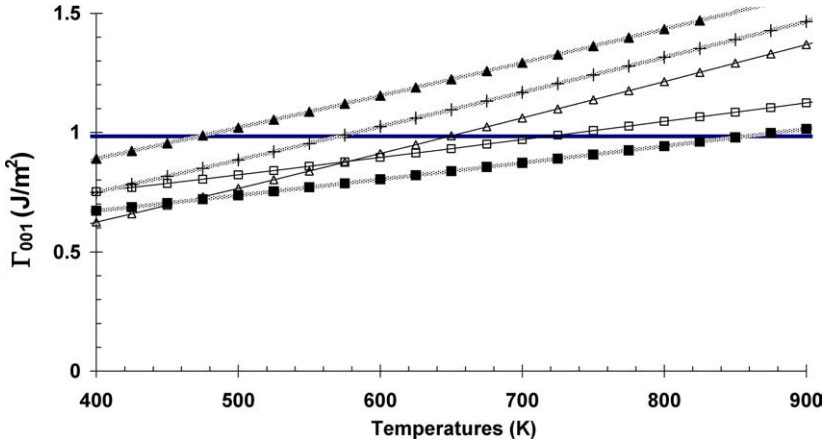

Fig. 4. Surface energy of the (001) surface of anatase–TiO_2 as a function of temperature for different coverages of H_2O and H_2S, $P_{H_2O} = 10^{-2}$ bar, and $P_{H_2S} = 1$ bar. (—) $\theta_{001} = 0.0$ molecule/nm^2; (□) $\theta_{001}^{H_2O} = 1.7$ H_2O/nm^2; (△) $\theta_{001}^{H_2O} = 3.5$; (■) $\theta_{001}^{H_2S} = 1.7$ H_2S/nm^2; (▲) $\theta_{001}^{H_2S} = 3.5$; (+) $\theta_{001}^{H_2O} = 1.7$ and $\theta_{001}^{H_2S} = 1.7$.

The surface energy diagram for low water pressure and P_{H_2S} around 1 bar shows that the sulfided state remains stable even at high temperature (Fig. 4). Under usual HDS working conditions, the (001) surface is sulfided. The hydroxyl coverage is 3.5 OH/nm^2, and the S coverage is 1.7 S/nm^2. The OH groups are of Ti_V-μ_1–OH types and the S species are Ti_V-μ_2–S types.

3.1.3. (110) surface

Although it was shown in [21] that this surface is not thermodynamically stable under usual working conditions, insights on its reactivity for H_2S are interesting as a comparison. Its reactivity versus water adsorption is high due to the presence of Ti_{IV} sites. Adsorption energies of dissociated water are between −138 and −109 kJ/mol. The adsorption energies of H_2S are again smaller (between −104 and −59 kJ/mol for θ_{110} in the range of 1.9 to 7.7 H_2S/nm^2) than those of water, whatever the coverage may be. Mixed coverages involving H_2S and H_2O are also less stable than pure water at the surface. As a consequence, under usual HDS conditions fixed by $P_{H_2O} = 0.01$ bar and $P_{H_2S} = 1$ bar, no sulfur species can be stabilized on the surface. Up to 610 K, the surface exhibits Ti_V–μ_1-OH and (Ti_V, Ti_{VI})–μ_2-OH groups. However, it must be underlined that for $P_{H_2O} = 0.01$ bar and for $P_{H_2S} = 100$ bar and for temperature around 600 K, the formation of μ_1-SH groups is favored. For $P_{H_2O} = 10^{-5}$ bar and a partial pressure of H_2S of 1 bar, the formation of μ_1-SH groups at 500 K is also enabled. Whereas the presence of S species is excluded for the (101) surface, reasonable changes in the working conditions may lead to sulfhydryl groups on the (110) surface due to its moderate activity. The corresponding local structure of the sulfided state is given in Fig. 5.

3.2. Effect of P_{H_2S} on the γ-Al_2O_3 surfaces

More detailed results obtained on the construction and properties of γ-Al_2O_3 surfaces can be found in Refs. [20,22].

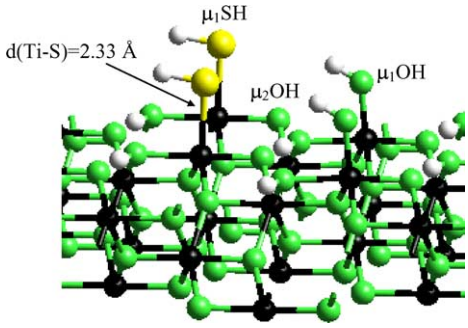

Fig. 5. Local structure of the (110) surface of anatase–TiO_2 for $\theta_{110}^{H_2O} = 1.9\ H_2O/nm^2$ and $\theta_{110}^{H_2S} = 1.9\ H_2S/nm^2$. (Same color coding as in Fig. 1.)

We have used most of these results which have been confirmed and extended within the PAW formalism [40]. No significant differences in the energetic results have been noted for our systems between the ultrasoft pseudopotentials used in [20,22] and the PAW formalism.

3.2.1. (110) surface

As already explained in [20–22], water molecules are strongly interacting with the (110) surface (Fig. 6). The H_2S adsorption energies are also higher than on anatase–TiO_2 surfaces, confirming the higher reactivity of the γ-alumina (110) surface. The value for one adsorbed H_2S molecule (−185 kJ/mol) is close to the one reported in [35] despite the different models used for γ-alumina. As for the anatase–TiO_2 (001) surface, the destabilization of S species as a function of coverage is rather high on this highly active surface. For a coverage between 1.5 and 7.5 H_2S/nm^2, the variation in adsorption energies is about 100 kJ/mol for γ-alumina, whereas it is about 140 kJ/mol for anatase–TiO_2 (001). However, in the case of γ-alumina, we do not find a configuration where the adsorption energy is more favorable for H_2S than for H_2O, even in the case of mixed coverages (Fig. 6). The consequence for the surface energy diagram is that for $P_{H_2O} \sim 0.01$ bar, $P_{H_2S} \sim 1$ bar, and T within 600–700 K, no chemically adsorbed S species is stabilized on the surface (Fig. 7a). The surface is covered by water between 2.96 and 4.44 H_2O/nm^2 and exhibits μ_1-OH and μ_2-OH groups.

Under specific conditions, H_2S can be adsorbed on this surface. For instance, keeping the water pressure at 0.01 bar, and increasing P_{H_2S} up to 70 bar stabilizes Al_{IV}–SH groups for temperatures higher than 850 K. Another possibility is to decrease P_{H_2O} down to 10^{-5} bar, and to keep $P_{H_2S} = 1$ bar: Al_{IV}–SH groups are then stabilized for $T > 600$ K (Fig. 7b). The local structure of the stable μ_1-SH group is depicted in Fig. 8. At this stage, it is important to underline that only rather high temperatures and very low P_{H_2O} stabilize the sulfidation of the surface. The μ_2-S species are always less stable by 11 kJ/mol, while the μ_3-S is even less stable by 35 kJ/mol. In the α-Al_2S_3 crystal structure [45], the Al–S distances of μ_2-S and μ_3-S are respectively 2.17 and 2.29 Å, whereas the optimized Al–S distances on the sulfided surface are 0.25 Å longer, which explains the destabilization of S-species versus SH groups.

3.2.2. (100) surface

The reactivity of this surface is significantly weaker, leading to a nonhydrated state under usual HDS conditions [20–22]. Adsorption energies for water are reported in Fig. 9, and the resulting surface energy diagram is given in Fig. 10. Actually, this surface behaves similarly as the (101) surface of anatase–TiO_2, except that the adsorption of H_2S (if it occurs) is dissociative (see inset of Fig. 9). The adsorption energy is low (about −55 kJ/mol for $\theta_{100}^{H_2S} = 2.1\ H_2S/nm^2$), and the destabilization occurs rapidly for higher H_2S coverages. Furthermore, the formation of a μ_3-S in substitution of a μ_3-O atom is less stable by 45 kJ/mol. Our calculated adsorption energy for the first H_2S molecule (−55 kJ/mol) differs from the result by Ionescu et al. (−37 kJ/mol) [35]. At variance with these authors, we find that H_2S is dissociated on the (100) surface. This discrepancy is due to the spinel-like structure used in [35] for the surface model, leading to an underestimation of the reactivity of the (100) surface sites.

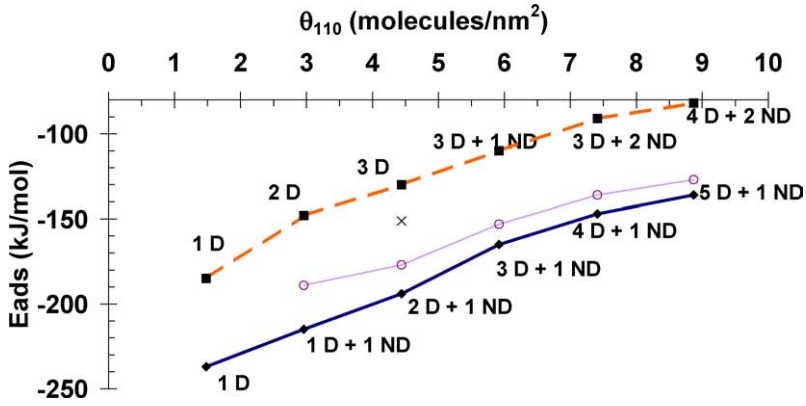

Fig. 6. Adsorption energies of H_2O (thick line) and H_2S (dashed line) on the (110) surface of γ-Al_2O_3 as a function of the coverage. (■) $\theta_{110}^{H_2S} = \theta_{110}$ and $\theta_{110}^{H_2O} = 0$ (pure H_2S); (×) $\theta_{110}^{H_2S} = 3\ H_2S/nm^2$ and $\theta_{110}^{H_2O} = 1.5\ H_2O/nm^2$; (○) $\theta_{110}^{H_2S} = 1.5$ and $\theta_{110}^{H_2O} \geqslant 1.5$; (◆) $\theta_{110}^{H_2S} = 0$ and $\theta_{110}^{H_2O} = \theta_{110}$ (pure H_2O). (D, dissociative adsorption; ND, nondissociative adsorption.)

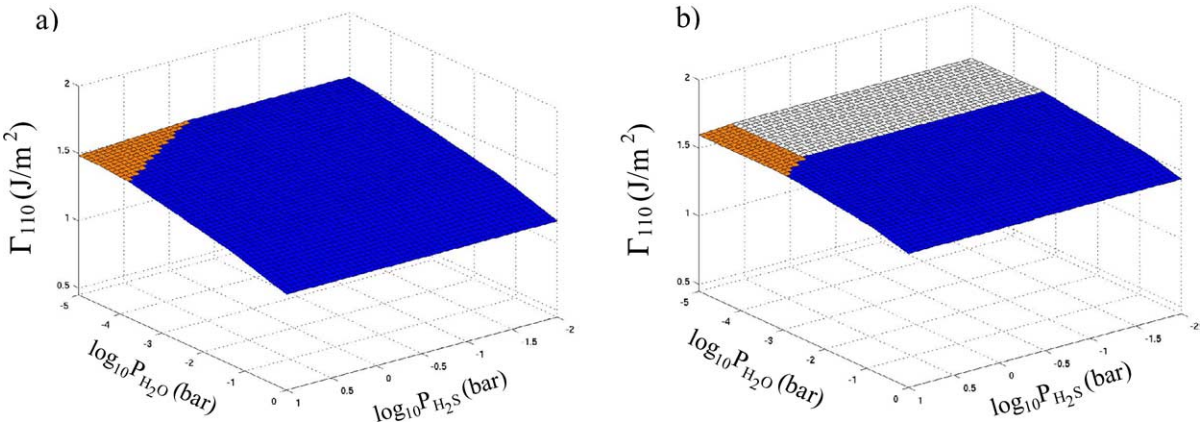

Fig. 7. Surface energy (Γ_{110}) diagram of γ-Al_2O_3 as a function of P_{H_2O} and P_{H_2S} for (a) $T = 700$ K and (b) $T = 900$ K. (Black domain, hydrated surfaces; gray domain, surfaces containing SH groups; light gray domain, surface without H_2O and H_2S.)

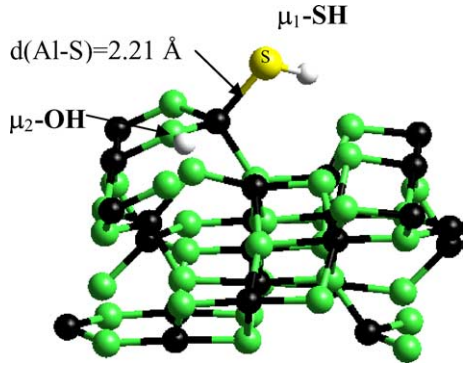

Fig. 8. Dissociative adsorption of H_2S on the (110) surface of γ-Al_2O_3 for $\theta_{110}^{H_2S} = 1.5$ H_2S/nm^2. (Black balls, Al; small gray balls, O; large gray balls, S; white balls, H.)

For usual HDS conditions given by P_{H_2O} around 0.01 bar, $P_{H_2S} = 1$ bar, and T between 600 to 700 K, no SH species is found on this surface. To stabilize such SH species at such temperature, the partial pressure of H_2S must be increased beyond realistic conditions, whatever P_{H_2O}.

3.3. Effect of P_{H_2} on the anatase–TiO_2 and γ-Al_2O_3 surfaces

To explore exhaustively the hydrodesulfurization conditions, the simulations must also take into consideration the reductive environment imposed by the high partial pressure of H_2 (up to 30 bar). Thus, it is necessary to investigate whether the exposed surfaces of the catalytic supports are modified by the presence of H_2, in competition with H_2O and H_2S. Indeed, H_2 may modify the type of surface species by increasing, for instance, the number of hydroxyls, by forming hydrides, or even by creating O vacancies. For that purpose, and for the most relevant surface states already determined in the previous sections, we study in what follows whether H_2 may be adsorbed in a molecular state, or in a dissociated state (either heterolytically or homolytically) or may remove O atoms. Given the complexity of the possible configurations, we focus on the most relevant ones.

3.3.1. Anatase–TiO_2 (101) surface

As we have shown in the previous sections, this surface is not hydrated and not sulfided for temperature and partial pressures of H_2O and H_2S close to HDS conditions. Table 1 gives the adsorption energies for H_2 in various configurations on the fully dehydrated (101) surface. The homolytic dissociation of one H_2 molecule on two μ_2-O basic sites is endothermic. The heterolytic dissociation on one μ_2-O sites and on Ti_V sites is even less favorable. The removal of one O atom from the surface leading to the formation of one water molecule is also highly endothermic, even if the water molecule formed remains adsorbed. As a consequence, the most favorable adsorbed configuration is the molecular state (Fig. 11) for which the adsorption energy is almost athermic (−3 kJ/mol). According to this weak adsorption energy, even at high partial pressure of H_2 (such as 30 bar), the surface energy diagram including the chemical potential of H_2 (not represented here) shows that no H_2 molecule is stable on the surface. The partial pressure of H_2 should be increased beyond realistic values to stabilize H_2 at the surface.

3.3.2. Anatase–TiO_2 (001) surface

The situation is more complex on this surface, because various hydrated and sulfided states are possible as a function of the reaction conditions (see Section 2). For the dehydrated and not sulfided surface (stable only at high temperature), the most favorable adsorption energy (−72 kJ/mol) is given by the homolytic dissociation represented in Fig. 12a. The stabilization is significantly stronger than for the (101) surface, due to the formation of H bonds when hydroxyls are formed. The adsorption energies for the other adsorption modes at low coverage are reported in Table 1. It is interesting to note that the heterolytic dissociation (Fig. 12b) is also exothermic. However, these adsorption energies remain smaller than those of H_2S (−184 kJ/mol) and H_2O. Using the chemical potential approach, this means that even for high P_{H_2} (such as 30 bar), the dissociative adsorption of H_2 cannot compete with H_2S and the partial pressure of H_2

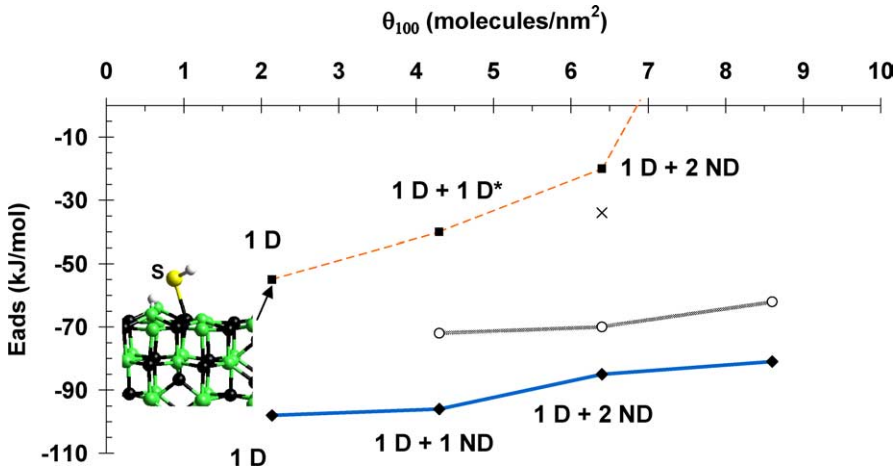

Fig. 9. Adsorption energies of H_2O (thick line) and H_2S (dashed line) on the (100) surface of γ-Al_2O_3 as a function of the coverage. (■) $\theta_{100}^{H_2S} = \theta_{100}$ and $\theta_{100}^{H_2O} = 0$ (pure H_2S); (×) $\theta_{100}^{H_2S} = 4.3$ H_2S/nm^2 and $\theta_{100}^{H_2O} = 2.1$ H_2O/nm^2; (○) $\theta_{100}^{H_2S} = 2.1$ and $\theta_{100}^{H_2O} \geqslant 2.1$; (◆) $\theta_{100}^{H_2S} = 0$ and $\theta_{100}^{H_2O} = \theta_{100}$ (pure H_2O). (D, dissociative adsorption; ND, nondissociative adsorption; D*, one H_2S molecule is dissociated by forming a μ_2-S species.) Inset with the same color coding as in Fig. 8.

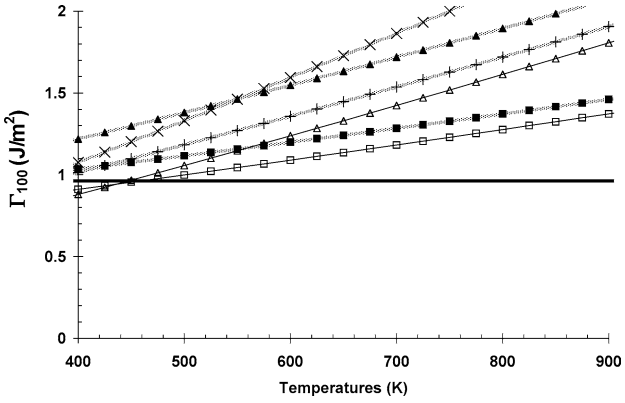

Fig. 10. Surface energy of the (100) surface of γ-Al_2O_3 as a function of temperature for different coverages of H_2O and H_2S, $P_{H_2O} = 10^{-2}$ bar, and $P_{H_2S} = 1$ bar. (—) $\theta_{100} = 0.0$ molecule/nm^2; (□) $\theta_{100}^{H_2O} = 2.1$ H_2O/nm^2; (△) $\theta_{100}^{H_2O} = 4.3$; (■) $\theta_{100}^{H_2S} = 2.1$ H_2S/nm^2; (▲) $\theta_{100}^{H_2S} = 4.3$; (+) $\theta_{100}^{H_2O} = 2.1$ and $\theta_{100}^{H_2S} = 2.1$; (×) $\theta_{100}^{H_2O} = 4.3$ and $\theta_{100}^{H_2S} = 2.1$.

should reach unrealistic values to allow the stabilization of H_2 versus H_2S on the (101) surface.

For higher coverages in H_2, the adsorption energy of H_2 decreases rapidly below −30 kJ/mol, remaining always far smaller than the adsorption energies of H_2O and H_2S. We have also tested some mixed coverages, such as 1.7 H_2O/nm^2 and 1.7 H_2S/nm^2, which lead to an average adsorption energy of −94 kJ/mol, significantly smaller than the mixed configuration involving H_2O and H_2S. As a consequence, in the presence of H_2S and even a slight amount of H_2O, most H species present at the surface of anatase are brought by H_2S or H_2O.

TPD experiments on anatase–TiO_2 pretreated at 773 K and 10^{-6} bar by Iwaki et al. [46] revealed that the highest H_2 desorption temperature is about 523 K at $P_{H_2} = 0.5$ bar. Such pretreatment conditions are sufficient to remove all H_2O molecules from the anatase surface. According to our simulations, under such conditions (excluding H_2S and H_2O), H_2 can be stabilized in a hemolytic dissociative state on the (001) surface and at 0.5 bar, and temperature lower than 580 K, which seems to be consistent with Iwaki's work.

3.3.3. γ-Al_2O_3 (100) surface

As we have shown in the previous section, this surface is not hydrated and not sulfided beyond 450 K for P_{H_2O} and P_{H_2S} corresponding to HDS conditions. As reported in Table 1 and similarly to the anatase–TiO_2 (101) surface, the most favorable adsorption mode for H_2 is the molecular state with a very weak adsorption energy of −4 kJ/mol (Fig. 13). As for the (101) surface of anatase–TiO_2, under a realistic partial pressure of H_2, no H_2 molecule remains adsorbed on the (100) surface of γ-alumina.

3.3.4. γ-Al_2O_3 (110) surface

As for the (001) surface of anatase–TiO_2, this surface is slightly more complex, since various hydrated states are found as a function of reaction conditions. In a first step, we calculate the adsorption energy of H_2 for the dehydrated surface. Table 1 shows that the heterolytic dissociation of a H_2 molecule is highly favored. The adsorption energy is −113 kJ/mol. Due to the presence of unsaturated Al_{III} sites, the heterolytic dissociation of H_2 on the μ_2-O sites and on the Al_{III} sites becomes favored versus the homolytic dissociation and molecular adsorption. This result confirms the high reactivity of the (110) surface also for H_2 activation, leading to the possible formation of a hydride ion together with a μ_2-OH group (inset of Fig. 14). This heterolytic dissociation may correspond to the highest TPD peak observed by Amenomiya [47] at 593 K and $P_{H_2} = 5.3 \times 10^{-2}$ bar.

Because the adsorption energy of H_2O is significantly higher (between −237 and −136 kJ/mol), H_2 competes for adsorption with H_2O, only if P_{H_2O} is very low. For

Table 1
Adsorption energies (in kJ/mol) of one H_2 molecule on anatase–TiO_2 and on γ-Al_2O_3 surfaces for $\theta^{H_2O} = 0$ and $\theta^{H_2S} = 0$

Surface	Homolytic dissociation	Heterolytic dissociation	Molecular adsorption	O vacancy creation[a]
Anatase (101)	+42	+86	−3	+95 (+H_2O)
Anatase (001)	−72	−26	−34	+28 (+2 OH)
γ-Al_2O_3 (100)	Highly endothermic	+128	−4	–
γ-Al_2O_3 (110)	+64	−113	−2	–

[a] The oxygen is removed from the surface site but remains adsorbed at the surface (through a water molecule or a hydroxyl group).

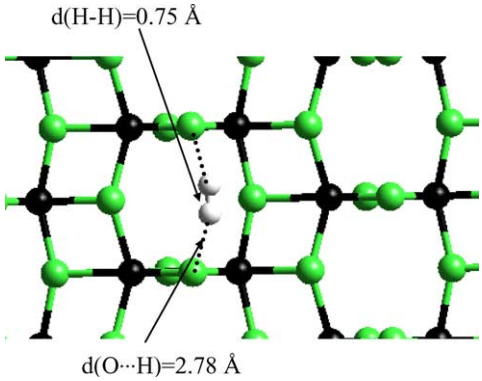

Fig. 11. Top view of the molecular adsorption of H_2 on the (101) surface of anatase–TiO_2 for $\theta^{H_2}_{101} = 1.3$ H_2/nm^2. (Same color coding as in Fig. 1.)

$P_{H_2O} = 10^{-2}$ bar, the surface energy diagram is not modified by the presence of H_2. For $P_{H_2O} = 10^{-5}$ bar, $P_{H_2S} = 1$ bar, $P_{H_2} = 30$ bar, H_2 is adsorbed with heterolytical dissociation for $T > 700$ K (Fig. 14). At higher coverages, some mixed configurations have been tested; however, we find that as soon as the Al_{III} sites are saturated, H_2 is molecularly adsorbed whatever the coverage may be.

4. Discussion

The sulfidation process of the two supports is governed by two main parameters: the intrinsic stability of the oxides with respect to sulfidation, and the reactivity of the exposed surfaces. Let us first consider the two following chemical reactions for the bulk reference systems (TiS_2 [44], Al_2S_3 [45]):

$$TiO_2 + 2H_2S \rightleftarrows TiS_2 + 2H_2O, \quad (7)$$

$$Al_2O_3 + 3H_2S \rightleftarrows Al_2S_3 + 3H_2O. \quad (8)$$

The Gibbs free enthalpies of reaction, ΔG_1 for (7) and ΔG_2 for (8), can be easily expressed as a function of T, P_{H_2S} and P_{H_2O} in a similar way as described in Section 2 for the surface. Using DFT results obtained on bulk cohesive energies, we find that at $T = 600$ K, $P_{H_2S} = 1$ bar, and $P_{H_2O} = 10^{-2}$ bar: $\Delta G_1 = +1.72$ eV and $\Delta G_2 = +3.18$ eV. As expected, this implies first that for both cases, the oxide phases are strongly stabilized versus the sulfide phases. The sulfidation can only occur partially under usual HDS conditions (at the surface). Then, it appears that TiO_2 is intrinsically more easily sulfided than Al_2O_3 ($\Delta G_1 < \Delta G_2$). Finally, for a given P_{H_2S}/P_{H_2O} ratio, a temperature increase implies a decrease of ΔG and enhances the probability of the sulfidation process.

Furthermore, the partial sulfidation of the support depends mainly on the specific reactivity of the exposed surfaces for H_2S. Table 2 summarizes the relevant conditions leading to the sulfidation of the different surfaces according to the results obtained in Section 3. As for the bulk system, at a given P_{H_2O}, high temperatures together with a sufficiently high P_{H_2S} are required to sulfide the surface. The simulations show that the sulfidation affinity is ordered as follows: (001) anatase > (110) γ-Al_2O_3 and (110) anatase ≫ (100) γ-Al_2O_3 and (101) anatase.

We conclude that the reactivity of the surfaces for H_2S is significantly different from their reactivity for H_2O [21,22]. Due to the higher intrinsic sulfidation affinity of TiO_2, the (001) surface of anatase is the most reactive one. In this case, as shown in Section 2, μ_2-S species are stabilized. The least reactive surfaces are the (101) anatase–TiO_2 and (100) γ-Al_2O_3 surfaces where H_2S is only weakly chemically adsorbed. The (110) anatase and (110) alumina surfaces exhibit intermediate behaviors, H_2S being dissociatively chemisorbed, and leading to the formation of sulfhydryl groups only when P_{H_2O} is very low (10^{-5} bar).

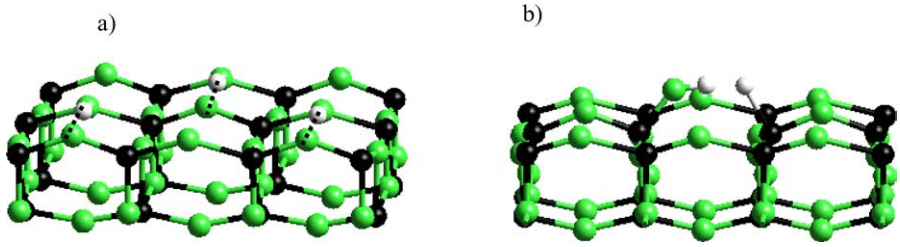

Fig. 12. (a) Homolytic dissociation and (b) heterolytic dissociation of H_2 on the (001) surface of anatase–TiO_2 for $\theta^{H_2}_{001} = 1.7$ H_2/nm^2. (Same color coding as in Fig. 1.)

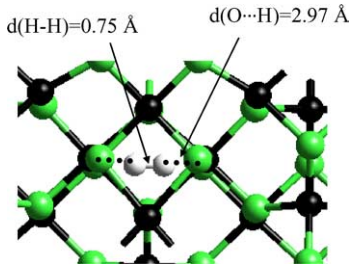

Fig. 13. Top view of the molecular adsorption of H_2 on the (100) surface of γ-Al_2O_3 for $\theta_{100}^{H_2} = 2.1$ H_2/nm^2. (Same color coding as in Fig. 8.)

As we have put forward in previous works [20–22], morphology effects are crucial for evaluating the surface species exposed by each nanoparticle of the support. According to the favorable H_2S adsorption on the (001) surface of anatase–TiO_2, a slight enhancement of the (001) facet is expected under HDS conditions (from 2 to 4% of the exposed area). Taking into consideration the Gibbs–Curie–Wulff equilibrium morphologies of the nanoparticles, the concentration of the different species (such as OH, SH groups, or S-atoms) is given in Table 3 for reaction conditions close to HDS. According to Section 3, the anatase–TiO_2 particles contain sulfur species under a wider range of (P_{H_2O}, P_{H_2S}, T) conditions than γ-Al_2O_3, which is sulfided under more restricted conditions. The sulfidation of γ-Al_2O_3 is possible only when the water partial pressure is drastically reduced (around 10^{-5} bar) to favor H_2S adsorption on the (110) surface. Furthermore, the types of S species present at the surface are different. On the (001) surface of anatase, the dissociative adsorption of H_2S leads to the formation of μ_2-S species, whereas for γ-alumina, the process occurring at very low P_{H_2O} leads to the formation of Al_{IV}–SH groups on the (110) surface. It must be underlined that for both supports, the surface sulfidation is enhanced at high temperatures. As shown in Table 3, at $T = 400$ K and $P_{H_2O} = 10^{-2}$ bar no sulfur species is present on the surfaces

Table 2
Conditions in P_{H_2O}, P_{H_2S}, and T inducing a partial sulfidation of the anatase–TiO_2 and γ-Al_2O_3 surfaces at fixed $P_{H_2} = 30$ bar

Support	(hkl) Surface	P_{H_2O} (bar)	P_{H_2S} (bar)	T (K)
Anatase–TiO_2	(101)	10^{-2}	Not realistic	
		10^{-5}		
	(001)	10^{-2}	1	600–850
		10^{-5}	10^{-3}	380–700
	(110)[a]	10^{-2}	100	∼600
		10^{-5}	1	420–530
γ-Al_2O_3	(100)	10^{-2}	Not realistic	
		10^{-5}		
	(110)	10^{-2}	70	850–1000
		10^{-5}	1	620–700

[a] For this surface, the adsorption of H_2 has not been investigated.

due to the preferential stabilization of water. This result furnishes a rational interpretation of the XPS study by Coulier et al. [7], who observed a perturbation of the 2p level of anatase Ti atoms, due to a partial sulfidation state at temperature above 673 K. According to our simulations, the sulfidation occurs through the formation of Ti_V–μ_2-S species on the (001) surface of anatase. For γ-alumina, the sulfidation is significantly less pronounced, and requires lower P_{H_2O}. Since precise values are seldom reported for P_{H_2O} during HDS operations, we cannot exclude that the sulfidation takes place if the γ-Al_2O_3 sample is submitted to a specific pretreatment temperature. However, it is important to underline the two distinct behaviors exhibited by TiO_2 and γ-Al_2O_3.

In the experimental literature, two types of chemisorption modes of H_2S are often reported on γ-Al_2O_3 [24,29,32], referred to as a dissociative mode and a nondissociative one. The earlier study based on adsorption isotherms by De Rosset et al. [48] estimated the isosteric heat of H_2S adsorption at −159 and −105 kJ/mol. Using similar techniques, Glass and Ross [24] showed that the heat of ad-

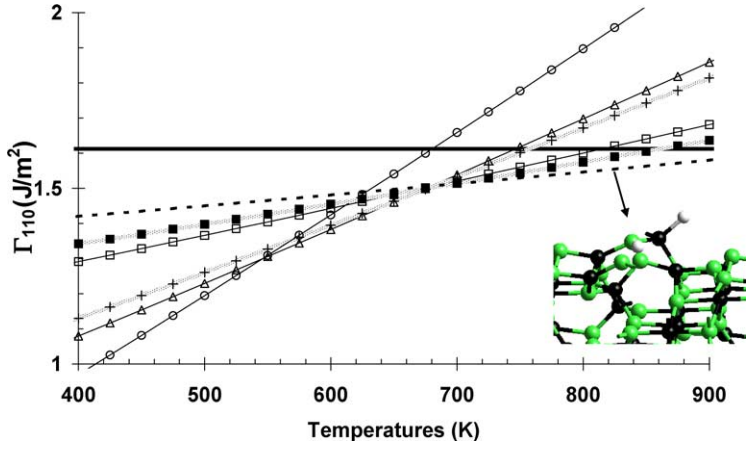

Fig. 14. Surface energy of the (110) surface of γ-Al_2O_3 as a function of temperature for different coverages of H_2O and H_2S, $P_{H_2O} = 10^{-5}$ bar, $P_{H_2S} = 1$ bar, and $P_{H_2} = 30$ bar. (—) $\theta_{110} = 0.0$ molecule/nm^2; (□) $\theta_{110}^{H_2O} = 1.5$ H_2O/nm^2; (△) $\theta_{110}^{H_2O} = 3.0$; (○) $\theta_{110}^{H_2O} = 4.4$; (■) $\theta_{110}^{H_2S} = 1.5$ H_2S/nm^2; (+) $\theta_{110}^{H_2O} = 1.5$ and $\theta_{110}^{H_2S} = 1.5$; (- - -) $\theta_{110}^{H_2} = 1.5$. (Inset with the same color coding as in Fig. 8.)

Table 3
Surface species concentrations (species/nm^2) at $P_{H_2S} = 1$ bar and $P_{H_2} = 30$ bar and for different morphologies

Support	P_{H_2O} (bar)	$T = 400$ K	$T = 600$ K	$T = 700$ K
TiO_2 eq. morp.				
(101) 96%	10^{-2}	0.67 [OH]	0.14 [OH] + 0.07 [S]	0.10 [OH] + 0.05 [S]
(001) 4%	10^{-5}	0.27 [OH] + 0.14 [S]	0.14 [OH] + 0.07 [S]	0.10 [OH] + 0.05 [S]
TiO_2 non eq.				
(101) 20%	10^{-2}	5.54 [OH]	2.77 [OH] + 1.38 [S]	2.77 [OH] + 1.38 [S]
(001) 80%	10^{-5}	2.77 [OH] + 1.38 [S]	2.77 [OH] + 1.38 [S]	2.77 [OH] + 1.38 [S]
γ-Al_2O_3 non eq.				
(100) 20%	10^{-2}	7.10 [OH]	7.10 [OH]	4.71 [OH]
(110) 80%	10^{-5}	7.10 [OH]	4.74 [OH]	1.18 [OH] + 1.18 [SH] or 1.18 [H]

Table 4
Surface sites of anatase–TiO_2 and γ-Al_2O_3 under HDS conditions (T = 600–700 K, $P_{H_2O} = 10^{-2}$ bar and $P_{H_2S} = 1$ bar, $P_{H_2} = 30$ bar)

Support	Surface	Brønsted and Lewis sites
Anatase	(101)	Ti_V, Ti_{VI}, μ_2-O, μ_3-O
	(001)	Ti_V–μ_2-OH; Ti_V, μ_2-O, μ_2-S
γ-Al_2O_3	(100)	Al_{IV}, Al_V, μ_3-O
	(110)	Al_{IV}–μ_1-OH, Al_V–μ_1-OH_2, (Al_{IV}, Al_V)–μ_2-OH, (Al_V, Al_V)–μ_2-OH, μ_3-OH; Al_{IV}, Al_{VI}, μ_2-O, μ_3-O

sorption of H_2S on γ-Al_2O_3, pretreated at 923 K, varies between −132 and −68 kJ/mol. More recently, Okamoto et al. [32] have shown from TPD spectra that two peaks are observed at ca. 400 and 560 K, corresponding to adsorption energies at −142 and −54 kJ/mol. Within the range of experimental and theoretical accuracies, these experimental data are consistent with our calculated results obtained in Section 3. On the γ-Al_2O_3 (110) surface, adsorption energies are varying between −184 and −80 kJ/mol (Fig. 6), while on the γ-Al_2O_3 (100) surface they are between −55 and −25 kJ/mol (Fig. 9). Furthermore, our simulations reveal that the dissociative mode and the nondissociative one contribute to the two adsorption regimes (Figs. 6 and 9). This implies that the two adsorption regimes observed are actually due to the two main exposed surfaces by the γ-Al_2O_3 nanoparticles. Hence, at low temperatures (400 K), the α-peak observed in TPD experiments [32] corresponds to H_2S adsorbed on the (100) surface. The shape of the peak is narrow, due to the small variation of H_2S adsorption energies on the γ-Al_2O_3 (100) surface (within 30 kJ/mol). The high-temperature β-peak (560 K) is assigned to H_2S adsorbed on the (110) surface. The width of the peak is larger, because of the wider range of adsorption energies on this surface (within 104 kJ/mol).

For HDS conditions, Table 4 summarizes the different types of Lewis and Brønsted sites present at the surface of the two supports. γ-Al_2O_3 exhibits a much greater variety of OH sites, whereas anatase–TiO_2 is partially sulfided. A detailed assignment of the stretching frequencies of OH groups was successfully carried out in [20–22].

For TiO_2 pretreated at 770 K (as investigated in [25]), our simulations reveal that the adsorption of H_2S in a dissociated state may remove H_2O previously adsorbed on the (001) surface and lead to the formation of μ_2-S and two μ_1-Ti_V–OH groups. The released water molecule may be adsorbed to Lewis sites located on the (101) surface (increasing the band intensity at 3675 cm^{-1}). The highest stretching frequency (3746 cm^{-1}) of one OH group after H_2S adsorption is similar to the one formed after H_2O. This is in qualitative agreement with the IR results of Travert et al. [25] showing that H_2S leads to a net increase of Brønsted acidity. As explained in Section 3, sulfhydryl groups can be formed on the (110) surface of anatase. The corresponding Ti_V–SH frequency is calculated at 2561 cm^{-1} (including anharmonicity corrections).

In the case of γ-Al_2O_3, Travert et al. investigated H_2S adsorption for two pretreatment temperatures. For the high temperature pretreated (1070 K) sample an increase of the OH band intensities is induced by H_2S adsorption. Because the OH coverage of γ-Al_2O_3 (110) surface is significantly reduced by such a high pretreatment temperature, and Al_{III} Lewis sites are available for the H_2S dissociative adsorption as shown in Section 3. The formation of Al_{IV}–SH groups together with new OH groups cannot be excluded. The corresponding SH-stretching frequency at 2518 cm^{-1} is lower than on the (110) anatase–TiO_2 surface, due to hydrogen bonds between the SH group and a neighboring O atom. As a consequence, we think that, for such a high pretreatment temperature of γ-Al_2O_3, a net increase of Brønsted acidity resulting from H_2S dissociative adsorption is expected. This is an intrinsic difference between γ-Al_2O_3 and anatase–TiO_2: the Brønsted acidity of anatase–TiO_2 is more sensitive to H_2S pressure than γ-Al_2O_3.

Regarding the effect of H_2 on the anatase–TiO_2 and γ-alumina surfaces, we find that the surface states (hydroxyls or S species) are not strongly modified by the high partial pressure of H_2. Due to the lower adsorption energies of H_2 on all surfaces, H_2 cannot compete for adsorption neither with H_2O (even if present in small amount) nor with H_2S. Only in the absence of these two species, H_2 can react with the (001) surface of anatase, and with the (110) surface of γ-alumina in a realistic range of P_{H_2}. In the former case, the thermodynamically favored homolytic dissociation leads to the formation of two hydroxyls. In the latter,

the heterolytic dissociation leads to Al_{III}–H and Al–μ_2-OH species. However, in both cases, an atmosphere free from H_2S (anatase–TiO_2) and H_2O (γ-alumina) is required to allow such a strong interaction of H_2 with the surface.

5. Conclusion

The present work has explored the effects of sulfo-reductive conditions on two supports relevant for HDS catalysts. Combining DFT calculations and a simple thermodynamic model, we put forward that under HDS conditions ($T = 600$–700 K, $P_{H_2O} \sim 10^{-2}$ bar, $P_{H_2S} \sim 1$–5 bar, and P_{H_2} up to 30 bar), anatase–TiO_2 can be partially sulfided whereas γ-Al_2O_3 cannot. On the one hand, this is due to the higher intrinsic sulfidability of anatase–TiO_2 versus γ-Al_2O_3. On the other hand, the (001) surface of anatase–TiO_2 exhibits a peculiar reactivity with H_2S leading to the formation of μ_2-S species together with OH groups. H_2S may thus increase the hydroxyls concentration on anatase–TiO_2. For γ-Al_2O_3, the formation of SH groups on the (110) surface is possible only if water is almost completely removed from the reaction medium (i.e., $P_{H_2O} < 10^{-5}$ bar). As a consequence, for moderate pretreatment temperatures, γ-Al_2O_3 Brønsted acidity is less sensitive to H_2S pressure than anatase–TiO_2. For higher pretreatment temperatures, γ-Al_2O_3 Brønsted acidity may be enhanced by H_2S pressure.

The adsorption of H_2 on surfaces of both supports reveals that its adsorption energy remains too low to compete with H_2S and H_2O, even at high H_2 pressures such as 30 bars. On γ-Al_2O_3, the heterolytic dissociation of H_2 is possible for $T > 700$ K and for $P_{H_2O} < 10^{-5}$ bar, leading to the formation of a hydride ion.

We expect that this ab initio determination of the surface states will allow a better control of the acidic properties of the two supports as a function of operating conditions. Moreover, this study provided us with the best possible basis to further investigate supported of MoS_2-based models of industrial HDS catalysts. Such as investigation will be reported in a near future.

Acknowledgments

The authors are grateful to M. Digne from IFP and to A. Travert, F. Maugé, and J.-C. Lavalley from the Université de Caen (France) for fruitful discussions. C. Arrouvel thanks also R. Scheichl from the University of Bath (UK) for his kind help in using the Matlab software. This work has been undertaken within the Groupement de Recherche Européen "Dynamique Moléculaire Quantique Appliquée à la Catalyse," a joint project of IFP-CNRS-TOTAL-Universität Wien.

References

[1] H. Topsøe, B.S. Clausen, F.E. Massoth, in: Hydrotreating Catalysis–Science and Technology, vol. 11, Springer, Berlin, 1996.
[2] R. Prins, in: Handbook of Heterogeneous Catalysis, vol. 4, Wiley–VHC, Weinheim, 1997.
[3] P. Euzen, P. Raybaud, X. Krokidis, H. Toulhoat, J.-L.L. Loarer, J.-P. Jolivet, C. Froidefond, in: Handbook of Porous Solids, vol. 3, Wiley–VCH, Weinheim, 2002.
[4] J. Ramirez, S. Fuentes, G. Díaz, M. Vrinat, M. Breysse, M. Lacroix, Appl. Catal. 52 (1989) 211.
[5] R.B. Quincy, M. Houalla, A. Proctor, D.M. Hercules, J. Phys. Chem. 93 (1989) 5882.
[6] K.Y.S. Ng, E. Gulari, J. Catal. 95 (1985) 33.
[7] L. Coulier, J.A.R. van Veen, J.W. Niemantsverdriet, Catal. Lett. 79 (2002) 149.
[8] V. Harlé, M. Vrinat, J.P. Scharff, B. Durand, J.P. Deloume, Appl. Catal. A 196 (2000) 261.
[9] E. Lecrenay, K. Sakanishi, T. Nagamatsu, I. Mochida, T. Susuka, Appl. Catal. B 18 (1998) 325.
[10] S. Dzwigaj, C. Louis, M. Breysse, M. Cattenot, V. Bellière, C. Geantet, M. Vrinat, P. Blanchard, E. Payen, S. Inoue, H. Kudo, Y. Yoshimura, Appl. Catal. B 41 (2003) 181.
[11] F. Luck, Bull. Soc. Chim. Belg. 100 (1991) 781.
[12] M. Breysse, J.L. Portefaix, M. Vrinat, Catal. Today 10 (1991) 489.
[13] G. Busca, H. Saussey, O. Saur, J.-C. Lavalley, V. Lorenzelli, Appl. Catal. 14 (1985) 245.
[14] Y. Araki, K. Honna, H. Shimida, J. Catal. 207 (2002) 361.
[15] P. Raybaud, J. Hafner, G. Kresse, S. Kasztelan, H. Toulhoat, J. Catal. 189 (2000) 129.
[16] H. Schweiger, P. Raybaud, G. Kresse, H. Toulhoat, J. Catal. 207 (2002) 76.
[17] P. Raybaud, M. Digne, R. Iftmie, W. Wellens, P. Euzen, H. Toulhoat, J. Catal. 201 (2001) 236.
[18] M. Digne, P. Sautet, P. Raybaud, H. Toulhoat, E. Artacho, J. Phys. Chem. B 106 (2002) 5155.
[19] X. Krokidis, P. Raybaud, A.-E. Gobichon, B. Rebours, P. Euzen, H. Toulhoat, J. Phys. Chem. B 105 (2001) 5121.
[20] M. Digne, P. Sautet, P. Raybaud, P. Euzen, H. Toulhoat, J. Catal. 211 (2002) 1–5.
[21] C. Arrouvel, M. Digne, M. Breysse, H. Toulhoat, P. Raybaud, J. Catal. 222 (2004) 152.
[22] M. Digne, P. Sautet, P. Raybaud, P. Euzen, H. Toulhoat, J. Catal. 226 (2004) 54.
[23] O. Saur, T. Chevreau, J. Lamotte, J. Travert, J.-C. Lavalley, J. Chem. Soc., Faraday Trans. 1 77 (1981) 427.
[24] R.W. Glass, R.A. Ross, J. Phys. Chem. 77 (1973) 2576.
[25] A. Travert, O.V. Manoilova, A.A. Tsyganenko, F. Maugé, J.C. Lavalley, J. Phys. Chem. B 106 (2002) 1350.
[26] H. Saussey, O. Saur, J.-C. Lavalley, J. Chem. Phys. 81 (1984) 261.
[27] D.D. Beck, J.M. White, C.T. Ratcliffe, J. Phys. Chem. 90 (1986) 3123.
[28] T.L. Slager, C.H. Amberg, Can. J. Chem. 50 (1972) 3416.
[29] A. Datta, R.G. Cavell, J. Phys. Chem. 89 (1985) 450.
[30] D. Wang, W. Qian, A. Ishihara, T. Kabe, Appl. Catal. A 224 (2002) 191.
[31] M. Ziolek, J. Kujama, O. Saur, J.C. Lavalley, J. Mol. Catal. A: Chem. 97 (1995) 49.
[32] Y. Okamoto, M. Oh-Hara, A. Maezawa, T. Imanaka, S. Teranishi, J. Phys. Chem. 90 (1986) 2396.
[33] A. Selloni, A. Vittadini, M. Grätzel, Surf. Sci. 402–404 (1998) 219.
[34] O. Maresca, A. Allouche, J.P. Aycard, M. Rajzmann, S. Clemendot, F. Hutschka, J. Mol. Struct. (Theochem) 505 (2000) 81.
[35] A. Ionescu, A. Allouche, J.-P. Aycard, M. Rajzmann, F. Hutschka, J. Phys. Chem. 106 (2002) 9359.

[36] J.P. Perdew, Y. Wang, Phys. Rev. B 45 (1992) 13244.
[37] G. Kresse, J. Hafner, Phys. Rev. B 49 (1994) 14251.
[38] G. Kresse, J. Furthmüller, Comput. Mater. Sci. 6 (1996) 15.
[39] http://cms.mpi.univie.ac.at/vasp/.
[40] G. Kresse, D. Joubert, Phys. Rev. B 59 (1999) 1758.
[41] B. Lindberg, J. Chem. Phys. 88 (1988) 3805.
[42] I.N. Senchenya, E. Garrone, P. Ugliengo, J. Mol. Struct. (Theochem) 368 (1996) 93.
[43] P. Ugliengo ANHARM; A program to solve numerically the monodimensional nuclear Schrödinger equation, unpublished.
[44] P. Ehrlich, Z. Anorg. Allg. Chem. 260 (1949) 1.
[45] B. Krebs, A. Schiemann, M. Läge, Z. Anorg. Allg. Chem. 619 (1993) 983.
[46] T. Iwaki, J. Chem. Soc., Faraday Trans. 1 79 (1983) 137.
[47] Y. Amenomiya, J. Catal. 22 (1971) 109.
[48] A.J. De Rosset, C.G. Finstrom, C.J. Adams, J. Catal. 1 (1962) 235.